HHS Public Access

Author manuscript

Am J Physiol Heart Circ Physiol. Author manuscript; available in PMC 2016 December 15.

Published in final edited form as:

Am J Physiol Heart Circ Physiol. 2015 December 15; 309(12): H2017–H2030. doi:10.1152/ajpheart.00353.2015.

Cardiac and mitochondrial dysfunction following acute pulmonary exposure to mountaintop removal mining particulate matter

Cody E. Nichols[1,2], **Danielle L. Shepherd**[1,2], **Travis L. Knuckles**[2,3], **Dharendra Thapa**[1,2], **Janelle C. Stricker**[2], **Phoebe A. Stapleton**[2,4], **Valerie C. Minarchick**[2,4], **Aaron Erdely**[4,5], **Patti C. Zeidler-Erdely**[4,5], **Stephen E. Alway**[1,2], **Timothy R. Nurkiewicz**[2,4], and **John M. Hollander**[1,2]

[1]West Virginia University School of Medicine, Division of Exercise Physiology, Morgantown, West Virginia

[2]Center for Cardiovascular and Respiratory Sciences, Morgantown, West Virginia

[3]West Virginia University, School of Public Health, Morgantown, West Virginia

[4]West Virginia University, Department of Physiology and Pharmacology, Morgantown, West Virginia

[5]National Institute for Occupational Safety and Health, Morgantown, West Virginia

Abstract

Throughout the United States, air pollution correlates with adverse health outcomes, and cardiovascular disease incidence is commonly increased following environmental exposure. In areas surrounding active mountaintop removal mines (MTM), a further increase in cardiovascular morbidity is observed and may be attributed in part to particulate matter (PM) released from the mine. The mitochondrion has been shown to be central in the etiology of many cardiovascular diseases, yet its roles in PM-related cardiovascular effects are not realized. In this study, we sought to elucidate the cardiac processes that are disrupted following exposure to mountaintop removal mining particulate matter (PM_{MTM}). To address this question, we exposed male Sprague-Dawley rats to PM_{MTM}, collected within one mile of an active MTM site, using intratracheal instillation. Twenty-four hours following exposure, we evaluated cardiac function, apoptotic indices, and mitochondrial function. PM_{MTM} exposure elicited a significant decrease in ejection fraction and fractional shortening compared with controls. Investigation into the cellular impacts

Address for reprint requests and other correspondence: J. Hollander, West Virginia Univ. School of Medicine, Div. of Exercise Physiology, Center for Cardiovascular and Respiratory Sciences, 1 Medical Center Dr., Morgantown, WV 26506 (jhollander@hsc.wvu.edu).

DISCLOSURES

No conflicts of interest, financial or otherwise, are declared by the authors.

AUTHOR CONTRIBUTIONS

Author contributions: C.E.N., T.L.K., P.A.S., T.R.N., and J.M.H. conception and design of research; C.E.N., D.L.S., T.L.K., D.T., J.C.S., P.A.S., V.C.M., A.E., and P.C.Z.-E. performed experiments; C.E.N. and D.L.S. analyzed data; C.E.N., D.T., S.E.A., T.R.N., and J.M.H. interpreted results of experiments; C.E.N. prepared figures; C.E.N. and J.M.H. drafted manuscript; C.E.N., D.L.S., T.L.K., D.T., P.A.S., A.E., P.C.Z.-E., S.E.A., T.R.N., and J.M.H. edited and revised manuscript; C.E.N., D.L.S., T.L.K., D.T., J.C.S., P.A.S., V.C.M., A.E., P.C.Z.-E., S.E.A., T.R.N., and J.M.H. approved final version of manuscript.

of PM_{MTM} exposure identified a significant increase in mitochondrial-induced apoptotic signaling, as reflected by an increase in TUNEL-positive nuclei and increased caspase-3 and -9 activities. Finally, a significant increase in mitochondrial transition pore opening leading to decreased mitochondrial function was identified following exposure. In conclusion, our data suggest that pulmonary exposure to PM_{MTM} increases cardiac mitochondrial-associated apoptotic signaling and decreases mitochondrial function concomitant with decreased cardiac function. These results suggest that increased cardiovascular disease incidence in populations surrounding MTM mines may be associated with increased cardiac cell apoptotic signaling and decreased mitochondrial function.

Keywords

mitochondria; cardiac function; particulate matter; apoptosis

NEW & NOTEWORTHY

We describe for the first time cardiac and mitochondrial dysfunction following an acute pulmonary exposure to a unique particulate matter, which arises from the process of mountain-top removal, common in surface mining operations. Our findings suggest enhanced cardiac risk for populations living in close proximity to mountaintop mining operations.

The world health organization estimates that 3.7 million premature deaths a year are attributed to ambient air pollution (75). While the lungs are the primary tissue impacted by air pollution exposure, more than 80% of these deaths are due to cardiovascular disease (75). Throughout the United States, decreased air quality correlates with adverse health effects, including negative cardiovascular end points (57, 60, 61, 64). Although chronic exposure to air pollution is the 13th leading cause of worldwide mortality (76), short-term particulate matter (PM) exposure has also been suggested to contribute to tens of thousands of deaths within the United States (60, 70c). Air pollution is a complex mixture of many compounds, including PM, and epidemiological data link PM concentration to adverse cardiovascular effects (84). PM itself is a heterogeneous mixture of particles that vary in size, chemical composition, and origin; nevertheless, persistent PM formation creates a near-universal inhalation exposure. Although PM exposure is widespread, the makeup of this material varies considerably based on origin and geographical region (70c). These differing compositions may play a distinct role in adverse cardiovascular end points associated with a specific geographic locale (22).

The United States is among the most active coal-producing countries in the world (28), and coal mining is projected to increase over the next 25 years (70a). The Appalachian region, which extends from southern New York to Mississippi and Georgia following the Appalachian Mountains, contains more than eight hundred active coal mines, accounting for 30% of US mining activity (70b). Due to its inherent less labor-intensive methods, surface mining is beginning to outnumber traditional underground mining two to one (70b). One popular, less labor-intensive method of surface mining is mountaintop removal mining (MTM), which utilizes explosives to remove the mountaintop, freeing underlying coal

seams, allowing easier extraction. Economically and ecologically, the technique is controversial, but few studies have begun to investigate the human health impacts in areas surrounding MTM sites. The PM generated by the MTM process contains toxicants that are environmentally biopersistent (55), suggesting potential for negative health effects.

Although the goal of industrial processes is to abate dust generation, fugitive dust from explosive treatment as well as combustion particles from heavy equipment create a unique PM (PM_{MTM}). Epidemiologically, health effects of coal mining have been outlined (81, 88), but, until recently, no comparisons had been drawn between areas surrounding underground and MTM sites. Studies have reported that PM_{MTM} causes an increase in chronic cardiovascular disease mortality rates among populations in close proximity to active MTM sites (28). However, the mechanisms underlying this observation are poorly understood. We have previously reported that acute pulmonary exposure to PM_{MTM} in rodents is linked to microvascular dysfunction in extrapulmonary tissue (36). However, studies on cardiac tissue have not been undertaken.

The mitochondrion has been implicated in the etiology of many cardiovascular diseases because of the crucial roles it plays within the cardiomyocyte. Among the central roles for the mitochondrion are the production of ATP requisite for cardiac contraction and relaxation as well as its contribution to the signals initiating cellular apoptosis. In vivo and in vitro analyses have revealed an increase in apoptosis in numerous tissues following PM exposure (2, 16, 85, 86). Two pathways reported to activate the apoptotic cascade include the extrinsic pathway via caspase-8 and the intrinsic pathway involving the mitochondrion. In the intrinsic pathway, opening of the mitochondrial permeability transition pore (mPTP) allows uncoupling of the electron transport chain, leading to mitochondrial dysfunction and formation of the apoptosome (31). In vitro evidence suggests that both extrinsic and intrinsic pathways are activated following PM exposure (20). Nevertheless, it is unclear whether acute PM_{MTM} exposure is associated with mitochondrial dysfunction or enhanced initiation of the apoptotic cascade.

The goals of the present study were to determine whether acute PM_{MTM} exposure is associated with cardiac and mitochondrial dysfunction and to elucidate whether these effects were associated with mitochondrial-associated apoptosis initiation with an emphasis on the cardiomyocyte. Our results suggest that acute PM_{MTM} exposure is associated with an increase in mitochondrial-driven apoptotic signaling, which may contribute to cardiac and mitochondrial dysfunction. These findings lend insight into the potential mechanisms underlying acute PM_{MTM} exposure effects in the heart.

MATERIALS AND METHODS

Experimental animals

The animal experiments in this study were approved by the West Virginia University Animal Care and Use Committee and conformed to the most current National Institutes of Health (NIH) *Guidelines for the Care and Use of Laboratory Animals* manual. Male Sprague-Dawley rats were housed in the West Virginia University Health Sciences Center animal facility. Rats were given access to a rodent diet and water ad libitum.

PM_{MTM} preparation

PM was collected on 35-mm, 5-μm pore size polytetrafluoroethylene fiber-backed filters (Whatman, Springfield Mill, UK) for 2–4 wk at two sites within 1 mile of an active MTM site. Particle storage and extraction from the filters following collection are consistent with previous reports (24). Briefly, filters were stored at room temperature (20–25°C) and ambient humidity (10–30%) before extraction. PM extraction was accomplished by gentle agitation in ultrapure water for 96 h. Particle suspension aliquots were then dried in a Speedvac (Savant, Midland, MI), and total particle weight was determined using a microbalance (Metler-Toledo, Columbus, OH).

Intratracheal instillation

Intratracheal instillation was performed according to the method of Brain et al. (4) as previously described (36, 45, 46, 49, 50). Briefly, following anesthesia with isoflurane, a ball needle attached to a 1-ml tuberculin syringe was inserted under the glottis into the trachea, and 300 μl of either vehicle (5% fetal bovine serum in phosphate-buffered saline) or vehicle with 300 μg of PM_{MTM} was instilled directly into the trachea. We have previously shown that this dose of PM_{MTM} partially impaired endothelium-dependent microvascular dysfunction (36). The PM characterization and resuspension were carried out as described previously (36).

Cardiac contractile function

Twenty-four hours following exposure, echocardiography was utilized to assess cardiac contractile function. For echocardiographic assessment, each rat was anesthetized in a knockdown box with inhalant isoflurane at 2.5% in 100% oxygen. Following anesthesia, ultrasound images were acquired with a 25-MHz linear array transducer using the Vevo2100 Imaging System (Visual Sonics, Toronto, Ontario, Canada). M-mode images were acquired by placing the transducer to the left of the sternum and obtaining an image at the mid-papillary muscle level. A gate was placed through the center of the short-axis B-mode image to obtain M-mode recordings of contractile parameters of the myocardium. Images were acquired using the highest possible frame rate (233–401 frames/s). Measurements obtained from left ventricular M-mode images included end-diastolic and end-systolic diameters and volumes, fractional shortening, ejection fraction, stroke volume, and cardiac output. All M-mode image measurements were calculated over three consecutive cardiac cycles and averaged.

Tissue preparation and compartment isolation

After cardiac contractile measurements were performed, rats were euthanized and hearts excised. Atrial and right ventricular tissues were removed, and left ventricular tissue was utilized for the studies. Cytosolic isolation was performed as previously described (77). Subsarcolemmal mitochondria (SSM) and interfibrillar mitochondria (IFM) subpopulations were isolated as previously described following the methods of Palmer et al. (54) with minor modifications by our laboratory (4, 5, 14, 15, 17, 18, 70, 77). Mitochondrial pellets were resuspended in KME buffer (100 mM KCl, 50 mM MOPS, and 0.5 mM EGTA pH 7.4) and

utilized for all analyses. Protein concentrations were determined by the Bradford method using bovine serum albumin as a standard (8).

TUNEL staining

Terminal dUTP nick-end labeling (TUNEL) was performed to detect apoptotic nuclei in tissue cross sections, as previously described (32, 74). Briefly, frozen tissue (10 μm thick) cross sections of left ventricle were mounted on charged microscope slides (Fisher Scientific, Pittsburgh, PA), air dried, and incubated overnight at 4°C with mouse anti-heavy chain cardiac myosin antibody (no. ab50967; Abcam, Cambridge, MA). Sections were then incubated with goat anti-mouse Cy5-conjugated secondary antibody (no. ab6563; Abcam), fixed with 4% paraformaldehyde, and permeabilized with 0.1% Triton X-100 in PBS at 4°C. Sections were incubated with the TUNEL reaction mixture (Roche Diagnostics, Indianapolis, IN) in a humidified chamber in the dark. The exclusion of the TdT enzyme in the TUNEL reaction mixture on one of the tissue sections on each slide was included as a negative control (Fig. 1*A*). Treatment of one tissue section on each slide with DNase I (Life Technologies, Carlsbad, CA) was included as a positive control (Fig. 1*B*). Sections were mounted and stained with a mounting medium containing DAPI (Vectashield; Vector Laboratories, Burlingame, CA) to observe nuclei. Slides were then visualized under a Zeiss Axio Imager Z2 (Carl Zeiss Microimaging, Thornwood, NY). The number of TUNEL- and DAPI-positive nuclei were counted, and the data were expressed as an apoptotic index, which was calculated as the percentage of TUNEL-positive nuclei relative to the total myonuclei (i.e., DAPI-positive nuclei) pool. The apoptotic index was determined from four nonoverlapping regions of each tissue cross section.

Histone ELISA

Cytoplasmic histone-associated DNA fragments related to apoptosis were quantified utilizing the Cell Death Detection ELISA^{PLUS} kit (no. 11774425001; Roche Diagnostics). This photometric enzyme immunoassay, which is used for the quantitative determination of mono- and oligonucleosomes after cell death, was carried out per the manufacturer's instructions.

Western blotting

SDS-PAGE was run on 4–12% gradient gels, as previously described (4, 5, 17, 18, 43, 70, 77). Relative amounts of activated caspase-3, -9, and -8 were determined using specific antibodies: anti-caspase-3 rabbit antibody (no. 3016-100; Biovision, Milpitas, CA), anti-caspase-9 rabbit antibody (no. 9665; Cell Signaling Technology, Danvers, MA), and anti-caspase-8 goat antibody (no. Sc6134; Santa Cruz Biotechnology, Dallas, TX). Relative amounts of B-cell CLL/lymphoma 2 (Bcl-2), Bcl-2-associated X protein (Bax), apoptosis protease-activating factor 1 (APAF-1), and cytochrome *c* were determined using specific antibodies: anti-Bcl-2 mouse antibody (no. sc-7382; Santa Cruz Biotechnology), anti-Bax rabbit antibody (no. ab32503; Abcam), anti-APAF-1 rabbit antibody (no. ab2000; Abcam), and anti-cytochrome *c* rabbit antibody (no. 4272; Cell Signaling Technology). Relative amounts of mitochondrial permeability transition pore constituents, adenine nucleotide translocase (ANT), voltage-dependent anion channel (VDAC), and cyclophilin D (CypD)

were determined using specific antibodies: anti-ANT goat antibody (no. sc-9300; Santa Cruz Biotechnology), anti-VDAC rabbit antibody (no. 4866; Cell Signaling Technology), and anti-CypD rabbit antibody (no. PA1-028; Affinity Bioreagents, Golden, CO). The secondary antibodies used included: goat anti-mouse IgG horseradish peroxidase (HRP) conjugate (no. 31430; Pierce Biotechnology, Rockford, IL), goat anti-rabbit IgG HRP conjugate (no. 10004301; Cayman Chemical, Ann Arbor, MI), and donkey anti-goat IgG HRP conjugate (no. sc-2020; Santa Cruz Biotechnology). Pierce Enhanced Chemiluminescence Western Blotting substrate (Pierce) was used to detect signal following the manufacturer's instructions. A G:Box Bioimaging system (Syngene, Frederick, MD) was used to assess autoradiographic signals. Data were captured using GeneSnap/GeneTools software (Syngene), and densitometry was analyzed using Image J software (National Institutes of Health, Bethesda, MD). Controls for protein loading included anti-GAPDH mouse antibody (no. ab8245; Abcam) for cytosolic analyses and anti-COXIV rabbit antibody for mitochondrial analyses (no. ab16056; Abcam).

Caspase activation

Caspase activities were assessed as previously described (77, 78). Briefly, whole left ventricular tissue was homogenized in the absence of a protease inhibitor cocktail to enable assessment of caspase-3, caspase-8, and caspase-9 activities. All of the activities were measured in a caspase activation buffer containing 4.8 mmol PIPES, 0.1 mmol EDTA, and 10% glycerol. For each enzyme activity assay, specific substrates were added: caspase-3, Ac-DEVD-AFC (Alexis Biochemicals, San Diego, CA); caspase-8, Ac-IETD-AMC (Alexis Biochemicals); and caspase-9, Ac-LEHD-AFC (Alexis Biochemicals). An aliquot (100 μg) of each sample was loaded with the appropriate substrate and allowed to incubate for 2 h in the dark at 37°C. Samples were read fluorometrically using a Flexstation 3 plate reader (Molecular Devices, Sunnyvale, CA). Fluorometric measurements were performed at excitation/emission wavelengths of 400 nm/505 nm and expressed in relation to protein content.

Immunoprecipitation

Isolated mitochondrial protein was incubated overnight with a primary anti-Bax rabbit antibody (no. ab32503; Abcam). Dynabeads Protein G superparamagnetic beads (product No. 10003D; ThermoFisher Scientific, Waltham, MA) were then added to the sample mixture and allowed to incubate for 1 h. After the beads were washed, the protein was eluted, heated, and run through SDS-PAGE as described above. Following SDS-PAGE, immunoblotting for relative amounts of Bcl-2 and Bax were accomplished as described above.

mPTP opening

mPTP opening was performed as previously described by measuring mitochondrial swelling spectrophotometrically (540 nm) and observing the decrease in light scattering (1, 77). Treatment of freshly isolated mitochondrial subpopulations with 100 μM tert-butyl hydroperoxide (t-BuOOH), 400 μM Ca^{2+}, and 10 mM succinate induced swelling and was followed using a Flexstation 3 plate reader (Molecular Devices). As an assay control, 1 μM cyclosporin A, a specific mPTP inhibitor, was added to the reaction mixture.

Mitochondria size and internal complexity

Size and complexity of the mitochondria were analyzed as previously described (18, 19) using a FACS Calibur flow cytometer equipped with a 15-MW 488-nm argon laser and 633-nm red diode laser (Becton and Dickinson, San Jose, CA). Each individual parameter (gating, size, and complexity) was measured using specific detectors and light sources (laser, photomultiplier tube). The dye MitoTracker Deep Red (no. M22426, Life Technologies), which passively diffuses into intact mitochondria, was used to selectively stain for mitochondria. Freshly isolated mitochondrial subpopulations were incubated with the dye, and 20,000 gated events were analyzed per sample. Gating parameters were established, and the forward scatter detector (FSC; 488 nm argon laser and diode detector) and side scatter detector (SSC; photomultiplier tube and 90° collection lens) were represented in FSC and SSC density plots. To represent size, FSC (logarithmic scale) geometric mean (arbitrary units) was used; to represent complexity, SSC (logarithmic scale) geometric mean (arbitrary units) was observed. All flow cytometry data collection was supervised by the West Virginia University Flow Cytometry Core Facility.

Electron microscopy

A section of left ventricle was cut and fixed in 3% glutaraldehyde in sodium cacodylate buffer for electron microscopy images. Briefly, sections were postfixed by incubation with a 1.0%/0.8% osmium tetroxide/potassium ferricyanide mixture (Electron Microscopy Science, Hatfield, PA), dehydrated through a graded series of ethanol solutions and acetone, and then embedded in Epon resin (SPI Supplies, Westchester, PA). Ultrathin sections (95 nm) were cut from the resulting blocks with a Leica EM UC7 ultramicrotome (Leica Biosystems, Buffalo Grove, IL) and then captured on 200 mesh copper electron microscopy grids. The sections were observed at 80 kV with a JEOL JEM-1010 electron microscope (JEOL USA, Peabody, MA) connected to an AMT XR611S-B (ORCA HR) digital camera driven by Image Capture Engine software (AMT, Woburn, MA) for image acquisition and analysis. All electron microscopy imaging was performed in conjunction with the West Virginia University Pathology Electron Microscopy Core Facility.

Mitochondrial respiration

State 3 and state 4 respiration rates were analyzed in freshly isolated mitochondrial subpopulations, as previously described (12, 13) with modifications by our laboratory (15, 17, 19, 70). Briefly, isolated mitochondrial subpopulations were resuspended in KME buffer, and protein content was determined by the Bradford method (8). Mitochondrial protein was added to respiration buffer (80 mM KCl, 50 mM MOPS, 1 mmol/l EGTA, 5 mmol/l KH_2PO_4, and 1 mg/ml BSA) and placed into a Gilson Chamber (Gilson, Middleton, WI) attached to a Yellow Springs Instruments 5300 biological oxygen monitor (Yellow Springs Instruments, Yellow Springs, OH). Maximal complex I-mediated respiration was initiated by the addition of glutamate (5 mM) and malate (5 mM). Data for state 3 (250 mM ADP) and state 4 (ADP limited) respiration were expressed as nanomoles of oxygen consumed per minute per milligram of protein.

Statistics

Means and SE were calculated for all data sets. A Student's *t*-test was employed to analyze differences between treatment groups using GraphPad Prism 5 software (GraphPad Software, La Jolla, CA). $P < 0.05$ was considered significant.

RESULTS

Cardiovascular function following PM_{MTM} exposure

Although overt cardiac dysfunction is not commonly an end point of PM exposure, acute PM exposure has been linked to cardiac stress (60); thus we began our investigation by evaluating cardiac function using echocardiography. Twenty-four hours following acute PM_{MTM} exposure, a significant increase in both end-systolic volume and diameter was observed, but no significant changes in end-diastolic parameters were noted (Table 1). Acute PM_{MTM} exposure led to decreases in ejection fraction and fractional shortening compared with control animals (Table 1).

Apoptotic signaling following PM_{MTM} exposure

Cardiac contractile dysfunction is associated with cell death; therefore, we determined whether acute PM_{MTM} exposure triggered apoptotic signaling in the heart. Cardiomyocytes from PM_{MTM}-exposed animals (Fig. 1*D*) displayed an increase in TUNEL-positive nuclei, which fluorescently labels DNA nicks, compared with control animals (Fig. 1*C*), suggestive of an increase in damage downstream of apoptotic signaling. Summary data for TUNEL-positive nuclei in both control and PM_{MTM}-exposed hearts can be seen in Fig. 1*E*. To confirm apoptotic initiation, we determined cytosolic histone content following PM_{MTM} exposure and found that exposure significantly increased histone concentrations (Fig. 1*F*).

Downstream signals of the apoptotic pathway may be differentially activated depending on the pathway of apoptosis initiated by a given stressor. Among the signaling pathways responsible for the apoptosis cascade are those driven by the extrinsic mechanism (caspase-8) as well as those driven by the intrinsic mechanism via the mitochondrion (caspase-9 and caspase-3) (56). No increase in the activity of caspase-8 was observed, suggesting that the extracellular pathway of apoptotic induction is not activated following PM_{MTM} exposure (Fig. 2*A*). In contrast, PM_{MTM} exposure enhanced the activity of both caspase-9 (Fig. 2*B*) and caspase-3 (Fig. 2*C*). These findings were supported by immunoblotting analysis of relative active caspase concentrations, which suggested an increase in caspase-3 (Fig. 2*F*) and caspase-9 (Fig. 2*E*) relative to control with no change in caspase-8 (Fig. 2*D*) following PM_{MTM} exposure. These findings indicate that the mitochondrion may play a role in the induction of cardiac apoptotic signals following acute PM_{MTM} exposure.

Apoptosome formation requires a number of molecular constituents, including APAF-1 and cytochrome *c* (83). Western blot analyses on the cytosolic fraction of left ventricular tissue from acute PM_{MTM}-exposed animals revealed a significant increase in APAF-1 content compared with control animals (Fig. 3*A*). Concurrently, there was an increase in the cytosolic cytochrome *c* content following acute PM_{MTM} exposure (Fig. 3*B*), confirming a

role of the mitochondrion in cardiac cell apoptotic signaling. Evaluation of mitochondrial cytochrome *c* content following acute PM_{MTM} exposure revealed a significant decrease in the SSM subpopulation (Fig. 3*C*) without impact on the IFM subpopulation (Fig. 3*D*). Taken together, these findings suggest an enhanced release of cytochrome *c* from cardiac SSM following acute PM_{MTM} exposure, which leads to apoptosome formation and mitochondrially driven apoptotic initiation.

To complement our apoptotic signaling analyses, we examined additional nonspecific cellular markers of apoptosis. BH3 proteins are a class of both pro- and antiapoptotic proteins found within the cytosol that are differentially expressed following cellular damage and act to either prevent or propagate apoptosis. Examination of the antiapoptotic protein Bcl-2 revealed a significant decrease following acute PM_{MTM} exposure (Fig. 4*A*). In contrast, no significant difference in the relative content of its antagonistic proapoptotic Bax protein was noted (Fig. 4*B*). The decrease in Bcl-2 led to a significant increase in the Bax:Bcl-2 ratio (Fig. 4*C*), suggesting a proapoptotic cellular environment. Bcl-2 and Bax are able to counteract each other's actions by forming dimers, either hetero or homo, to complete their anti- or proapoptotic activities. Therefore, it is the dimerization of these proteins that suggests mitochondrial apoptotic signaling. Immunoblotting for Bax following immunoprecipitation with an anti-Bax antibody indicated that there is an increase in Bax:Bax dimerization following exposure (Fig. 4*E*). When investigating the Bax:Bcl-2 dimerization, we observed no significant difference in the levels of Bcl-2 following pulldown with Bax in the animals exposed to PM_{MTM} (Fig. 4*D*). These results led us to observe an increase in the proapoptotic Bax:Bax homodimerization, compared with the antiapoptotic Bax:Bcl-2 heterodimerization following exposure to PM_{MTM} (Fig. 4*F*). These data further suggest that cardiac mitochondrial apoptotic signaling is increased following pulmonary PM_{MTM} exposure.

mPTP opening propensity

Mitochondrial-initiated apoptotic signaling is associated with the opening of the mPTP (42). We investigated mPTP opening propensity by inducing mitochondrial swelling using an exogenous oxidant (t-BuOOH). When the mPTP is open, the space that is occupied by the mitochondrial matrix is increased, and the time to V_{max} represents the rate of pore opening. Relative absorbance plots are presented for mPTP opening in SSM (Fig. 5*A*) and IFM (Fig. 5*C*). Each plot includes control, acute PM_{MTM} exposure, and an internal control consisting of cyclosporin A treatment, which limits mPTP opening. In general, IFM displayed greater times to V_{max} compared with SSM (Fig. 5, *B* and *D*; open bars), which is in agreement with other reports (1, 77). The time to V_{max} was significantly decreased in the SSM subpopulation following acute PM_{MTM} exposure (Fig. 5*B*). In contrast, mPTP opening propensity was not significantly altered in IFM following acute PM_{MTM} exposure (Fig. 5*D*). These results suggest that mPTP opening propensity is enhanced following acute PM_{MTM} exposure only in the SSM subpopulation, and, as a result, SSM are more susceptible to oxidant-induced apoptotic stimuli.

mPTP opening constituents

Because of the observed enhanced mPTP opening propensity, we determined whether putative constituents of the pore were affected following acute PM_{MTM} exposure. Specifically, we assessed the contents of ANT, VDAC, and CypD in both mitochondrial subpopulations. Acute PM_{MTM} exposure induced no change in VDAC (Fig. 6, *A* and *B*) or ANT (Fig. 6, *C* and *D*) in either mitochondrial subpopulation. In contrast, an increase in the levels of the regulatory subunit CypD was noted in the SSM (Fig. 6*E*) following acute PM_{MTM} exposure with no significant change in the IFM (Fig. 6*F*). These results indicate an increase in the CypD content in the SSM following acute PM_{MTM} exposure, which may contribute to the increased pore opening propensity.

Mitochondrial subpopulation morphology

mPTP opening is associated with morphological changes to the mitochondrion (31). To assess the impact of acute PM_{MTM} exposure on mitochondrial morphology, we utilized flow cytometry to determine relative size and internal complexity, as previously described (15, 17–19, 77). Using this approach, we have reported that SSM tend to be larger and more complex than IFM (15, 17, 18, 77), and data from the present study are in agreement with these reports (Fig. 7, *A* and *B*; open bars). In both the SSM and IFM, there were significant decreases in forward scatter (size) (Fig. 7*A*) and side scatter (internal complexity) (Fig. 7*B*) following acute PM_{MTM} exposure. The results were surprising and indicate that both the SSM and IFM were smaller and had decreased internal complexity following acute PM_{MTM} exposure, suggesting that mitochondrial morphology may be affected in both subpopulations. Qualitative assessment of electron micrographs of left ventricular tissues from control (Fig. 7*C*) and exposed animals (Fig. 7*D*) indicated that mitochondria were smaller following exposure, further supporting the data presented in Fig. 7*A*.

Mitochondrial respiratory function

Mitochondrial dysfunction is frequently concomitant with increased apoptotic signaling; therefore, we determined the respiratory capacity following acute PM_{MTM} exposure through evaluation of state 3 and state 4 respiration rates. Representative respiratory plots for the SSM and IFM can be seen in Fig. 8, *A* and *C*, respectively. We observed a significant decrease in state 3 respiration (active) following acute PM_{MTM} exposure in both the SSM (Fig. 8*B*) and IFM (Fig. 8*D*). No significant changes in the state 4 respiration, or resting respiration rate, in either subpopulation were noted following acute PM_{MTM} exposure. These findings suggest that acute PM_{MTM} exposure elicits disruption to respiratory capacity in both mitochondrial subpopulations.

DISCUSSION

Acute and chronic PM inhalation exposure contributes to and exacerbates cardiovascular disease and mortality (21, 70c). Within the Appalachian region, MTM activity creates a unique exposure, which, combined with mining longevity, may contribute to increased mortality from chronic diseases. Although epidemiological data are convincing, the underlying mechanisms responsible for increased morbidity following PM_{MTM} exposure are relatively unexplored. Utilizing an acute pulmonary exposure model, we investigated the

effects of acute PM_{MTM} exposure on cardiovascular function and metabolic disposition. Our data reveal decreases in cardiac pump function concomitant with increased mitochondria-driven apoptotic signaling and decreased mitochondrial respiratory function.

Particle composition varies by region in the US, and this variability may underlie health disparities for a given geographical region. Characterization of the particles utilized in this study indicated elements and sizes similar to those resulting from the combination of mineralogical materials, as well as engine exhaust emission (36). MTM utilizes blasting, crushing, and grinding of materials, which are commonly accomplished and transported by heavy machinery burning off-road diesel fuel. Validation of the PM was accomplished in another study highlighting natural and exhaust emissions, primarily geological, surrounding opencast mines similar to MTM (35). The dominant size range was ultrafine to 0.2 μm, based on mass measurement, and the principal particle composition was likely crustal with a bulk of particles appearing anthropogenic in origin (79). Previous elemental analyses support the notion that the bulk of the particle was from crustal sources (36). Further confirmation of composition was obtained by comparing PM from MTM sites and non-MTM sites and observing crustal material enriched within the surface mining samples by factors greater than 10 (39). These authors concluded that the PM was similar to coal dust and crustal material with the presence of local combustion sources. The authors also suggested that, because of the nature of the landscape surrounding the mines (steep valleys with lower wind speeds and less vertical mixing), there would be less PM transport, creating an increase in the inhaled deposited lung deposition and greater health effects (40). Whether or not these elements and observations are consistent with our observations remain to be determined in future experiments.

Although extrapulmonary toxicological effects are well documented, the mechanisms of toxicity are still under considerable debate. Three potential hypotheses have been advanced to explain extrapulmonary effects: *1*) a systemic inflammatory response that is initiated in the lung, *2*) translocation of the PM to extrapulmonary tissue, and *3*) neural effects (9, 23). Studies in both murine and human models have identified proinflammatory markers in the circulation of exposed subjects, providing evidence that a pulmonary insult may stimulate a systemic inflammatory response (7, 33, 58, 62, 63, 68, 71, 73), which may contribute to downstream cardiovascular effects (47, 51). Data also exist suggesting PM translocation from the lung to the affected tissues (26, 38, 52, 53, 67). Pulmonary exposure damages lung epithelium, increasing permeability and enabling PM penetration from the gaseous exchange region, leading to escape into the circulation with subsequent impact on extrapulmonary tissues (48, 65). Finally, PM exposure may interfere with neuronal signaling and cardiac autonomic dysfunction following exposure (10, 11, 59). Although the hypotheses are scientifically independent, the mechanisms are not mutually exclusive and may overlap, propagating activation of additional mechanisms. Although these mechanisms have not been explored following PM_{MTM} exposure, acute exposure to other PM has implicated a systemic inflammatory response (44). This question is not experimentally addressed in this study, but it is a crucial concept in fully understanding the interaction between pulmonary damage and extrapulmonary toxicity.

Acute PM exposure has been shown to contribute to cardiovascular morbidity and mortality. To investigate the cardiac contractile response following acute PM_{MTM} exposure, we utilized echocardiography and observed decreases in ejection fraction and fractional shortening, which were associated with increases in both end-systolic volume and diameter. One study investigating the effect of diesel exhaust particle inhalation exposure on cardiac function reported similar decreases in fractional shortening, yet this functional decrease was due to diastolic effects with an increase in end-diastolic diameter (82). Similarly, decreased fractional shortening following PM exposure was identified in senescent mice (69). Prenatal PM exposure reduced fractional shortening (30) and a chronic model of PM exposure decreased ejection fraction (80), demonstrating the detrimental role PM exposure plays in the progression of heart disease. Following PM exposure, overt cardiac dysfunction is not commonly observed in humans; however, cardiac remodeling occurs, indicating cardiac stress (72). Our results suggest conditions of early cardiac stress and alteration which, if maintained, may contribute to the onset and progression of cardiovascular disease.

To identify the cellular mechanisms contributing to cardiac contractile dysfunction following PM exposure, we focused on apoptotic signaling, the role of which has not been widely investigated in PM toxicology. Research into histological changes following oil combustion-derived, fugitive emission PM exposure indicated no change in cardiac cell apoptosis in a chronic model (37). It is unclear why these results differ from those in the present study, but it may be a function of differences in particle composition or a transient increased response, which ultimately triggers compensatory mechanisms to attenuate cell death. In addition, the activation of caspase cascades is a critical step in the induction of apoptosis, and our study identified increased cardiac caspase activity following PM_{MTM} exposure. Activation of both caspase-8 and -9 in the lung following PM exposure has been reported (29). In the present study, activation of caspase-3 and -9 suggested a mitochondrial role in apoptotic signaling associated with PM_{MTM} exposure. Additional studies are needed to determine whether these effects are specific to the cardiomyocyte. Interestingly, differences in absolute changes following PM_{MTM} exposure were observed between the TUNEL staining and the caspase activity analyses, in which TUNEL staining revealed a greater overall change compared with caspase activation. It should be pointed out that the TUNEL measurements were performed by staining specifically for cardiomyocytes, whereas the caspase activities were conducted on whole heart tissue, which may have diluted the overall absolute change. Furthermore, TUNEL analyses tend to be more sensitive in terms of absolute detection resolution.

The mPTP is considered a key nodal point in mediating cardiac dysfunction and cellular death. Pore opening enables release of proapoptotic proteins, including cytochrome *c*. Our study revealed increased propensity for mPTP opening specifically in the SSM following PM_{MTM} exposure. Although the constituents of the mPTP have been debated, CypD has been regarded as the regulatory subunit of the pore and necessary for pore opening (3). Our study revealed no difference in the content of putative pore constituents VDAC and ANT, yet we observed a significant increase in CypD content in the SSM following PM_{MTM} exposure. These data support a hypothesis of increased pore opening propensity specific for

the SSM following PM_{MTM} exposure. Differential subpopulation responses to apoptotic stimuli are consistent with other pathological models (1, 77).

Many studies indicate that mitochondrial spatial location may be associated with a specific response to pathological stimuli (34). Two spatially distinct mitochondrial subpopulations have been noted in the myocyte: SSM, which reside below the cell membrane, and IFM, which exist between the myofibrils. In the present study, SSM displayed increased apoptotic propensity following PM_{MTM} exposure. In contrast, both mitochondrial subpopulations displayed decreased active respiration rates after PM_{MTM} exposure. These findings indicate that, following PM_{MTM} exposure, there could potentially be a spatial component to metabolic insult. Furthermore, these data suggest that SSM are impacted to a greater extent by PM_{MTM} exposure, and, on the basis of their spatial position, we speculate that the primary source of cellular stress comes from outside the sarcolemma. SSM act as a protective barrier to the cell interior, maintaining permissive oxygen levels and the resulting cellular milieu (41, 66). We theorize that the impact to SSM supports the hypothesis that a pulmonary particle insult stimulates a systemic response, such as inflammation, which affects the cell at its periphery. It has been indicated that mitochondrial subpopulations can communicate across the cell, providing a platform for mitochondrial synchronization (87). The degree of interaction between these two subpopulations is of debate, but one hypothesis indicates that the innermost SSM and the outermost IFM are connected through mitochondrial filaments enabling metabolic coupling (66). If such a scenario were to exist, one could hypothesize that a significant insult at the SSM could stimulate dysfunction to the IFM.

In this study, we chose to use an acute exposure to PM_{MTM} using intratracheal instillation at a dose that would be similar to an accumulated dose over 1.7 yr. This dose was based on ambient recorded concentrations of 8.3 $\mu g/m^3$ and a minute ventilation of 200 ml/min with an estimated deposition fraction of 0.2 and was chosen because previous effects have been observed (36). Given that our model resembles a young, healthy population, our findings may be of even greater significance to older populations and populations with preexisting conditions. It should be noted that other methods of pulmonary exposure (e.g., inhalation), as well as a chronic model, may be more translationally relevant. This may be particularly applicable for heart failure, which can be influenced by mitochondrial dysfunction through bioenergetic deficit and myocyte apoptosis, both of which contribute to contractile dysfunction and cardiomyocyte loss. Because of the limited mass of PM_{MTM} particle collected, more demanding exposure approaches were not possible. Also because of the limited particle mass, elemental analysis was not undertaken; thus conclusions between elements and their contribution to the reported observations were not drawn. Indeed, future studies should employ inhalation exposure and in-depth elemental analysis to couple effects with a specific toxicant. Nevertheless, investigations into the acute effects of PM_{MTM} exposure are not without value, as they provide insight into the potential toxicological mechanisms elicited by PM_{MTM} exposure.

Although the current study is aimed at the populations proximal to MTM sites, our findings could provide a broader impact on our understanding of cardiovascular toxicology. The data presented in this manuscript show for the first time that exposure to PM_{MTM} induces cardiac

dysfunction concomitant with increased mitochondrial-associated apoptotic signaling and decreased mitochondrial function. Furthermore, our findings suggest that there is a spatial component to this dysfunction, as evidenced by differential effects to spatially distinct mitochondrial subpopulations.

Acknowledgments

We thank Caroll McBride, Dr. Katherine Brundage, Dr. Christopher Cuff, Dr. Amanda Ammer, and the West Virginia University Flow Cytometry Core, the West Virginia University Imaging Core, and the West Virginia University Animal Models of Imaging Core. We thank Dr. James Coad, Rebecca Radabaugh, and the West Virginia University Pathology and Electron Microscopy Core Facility.

GRANTS

This work was supported by the National Institute of Diabetes and Digestive and Kidney Diseases Grant DP2DK083095 (J. M. Hollander), the WVU CTSI (NIH U54GM104942) (J. M. Hollander), and ES015022 (T. R. Nurkiewicz). This work was supported by NSF award Nos. 1003907 and DGE-1144676 (T. R. Nurkiewicz). Cody Nichols is a recipient of an Integrative Graduate Education and Research Traineeship Program (DGE-1144676) and also a recipient of an American Heart Association Predoctoral Fellowship (AHA 13PRE16850066). Danielle Shepherd is a recipient of an NIH Predoctoral Fellowship (T32HL090610) and also an American Heart Association Predoctoral Fellowship (14PRE19890020). Phoebe Stapleton is a recipient of a postdoctoral fellowship (NIH F32 ES023435) and an NIH Career Development award (NIH K99 ES024783). Valerie Minarchick is also a recipient of an Integrative Graduate Education and Research Traineeship Program (DGE-1144676). Core facilities were supported by NIH P30RR031155, NIH P20 RR016440, NIH P30 GM103488, and NIH S10 RR026378.

References

1. Adhihetty PJ, Ljubicic V, Menzies KJ, Hood DA. Differential susceptibility of subsarcolemmal and intermyofibrillar mitochondria to apoptotic stimuli. Am J Physiol Cell Physiol. 2005; 289:C994–C1001. [PubMed: 15901602]
2. Astort F, Sittner M, Ferraro SA, Orona NS, Maglione GA, De la Hoz A, Tasat DR. Pulmonary inflammation and cell death in mice after acute exposure to air particulate matter from an industrial region of Buenos Aires. Arch Environ Contam Toxicol. 2014; 67:87–96. [PubMed: 24327098]
3. Baines CP, Kaiser RA, Purcell NH, Blair NS, Osinska H, Hambleton MA, Brunskill EW, Sayen MR, Gottlieb RA, Dorn GW, Robbins J, Molkentin JD. Loss of cyclophilin D reveals a critical role for mitochondrial permeability transition in cell death. Nature. 2005; 434:658–662. [PubMed: 15800627]
4. Baseler WA, Dabkowski ER, Jagannathan R, Thapa D, Nichols CE, Shepherd DL, Croston TL, Powell M, Razunguzwa TT, Lewis SE, Schnell DM, Hollander JM. Reversal of mitochondrial proteomic loss in Type 1 diabetic heart with overexpression of phospholipid hydroperoxide glutathione peroxidase. Am J Physiol Regul Integr Comp Physiol. 2013; 304:R553–R565. [PubMed: 23408027]
5. Baseler WA, Dabkowski ER, Williamson CL, Croston TL, Thapa D, Powell MJ, Razunguzwa TT, Hollander JM. Proteomic alterations of distinct mitochondrial subpopulations in the type 1 diabetic heart: contribution of protein import dysfunction. Am J Physiol Regul Integr Comp Physiol. 2011; 300:R186–R200. [PubMed: 21048079]
7. Becher R, Bucht A, Ovrevik J, Hongslo JK, Dahlman HJ, Samuelsen JT, Schwarze PE. Involvement of NADPH oxidase and iNOS in rodent pulmonary cytokine responses to urban air and mineral particles. Inhal Toxicol. 2007; 19:645–655. [PubMed: 17510837]
8. Bradford MM. A rapid and sensitive method for the quantitation of microgram quantities of protein utilizing the principle of protein-dye binding. Anal Biochem. 1976; 72:248–254. [PubMed: 942051]
9. Brook RD, Rajagopalan S, Pope CA 3rd, Brook JR, Bhatnagar A, Diez-Roux AV, Holguin F, Hong Y, Luepker RV, Mittleman MA, Peters A, Siscovick D, Smith SC Jr, Whitsel L, Kaufman JD. American Heart Association Council on Epidemiology and Prevention, Council on the Kidney in Cardiovascular Disease, and Council on Nutrition, Physical Activity and Metabolism. Particulate

matter air pollution and cardiovascular disease: An update to the scientific statement from the American Heart Association. Circulation. 2010; 121:2331–2378. [PubMed: 20458016]

10. Carll AP, Haykal-Coates N, Winsett DW, Hazari MS, Ledbetter AD, Richards JH, Cascio WE, Costa DL, Farraj AK. Cardiomyopathy confers susceptibility to particulate matter-induced oxidative stress, vagal dominance, arrhythmia and pulmonary inflammation in heart failure-prone rats. Inhal Toxicol. 2015; 27:100–112. [PubMed: 25600220]
11. Carll AP, Hazari MS, Perez CM, Krantz QT, King CJ, Haykal-Coates N, Cascio WE, Costa DL, Farraj AK. An autonomic link between inhaled diesel exhaust and impaired cardiac performance: insight from treadmill and dobutamine challenges in heart failure-prone rats. Toxicol Sci. 2013; 135:425–436. [PubMed: 23872579]
12. Chance B, Williams GR. Respiratory enzymes in oxidative phosphorylation. I. Kinetics of oxygen utilization. J Biol Chem. 1955; 217:383–393. [PubMed: 13271402]
13. Chance B, Williams GR. Respiratory enzymes in oxidative phosphorylation. VI. The effects of adenosine diphosphate on azide-treated mitochondria. J Biol Chem. 1956; 221:477–489. [PubMed: 13345836]
14. Croston TL, Shepherd DL, Thapa D, Nichols CE, Lewis SE, Dabkowski ER, Jagannathan R, Baseler WA, Hollander JM. Evaluation of the cardiolipin biosynthetic pathway and its interactions in the diabetic heart. Life Sci. 2013; 93:313–322. [PubMed: 23872101]
15. Croston TL, Thapa D, Holden AA, Tveter KJ, Lewis SE, Shepherd DL, Nichols CE, Long DM, Olfert IM, Jagannathan R, Hollander JM. Functional deficiencies of subsarcolemmal mitochondria in the type 2 diabetic human heart. Am J Physiol Heart Circ Physiol. 2014; 307:H54–H65. [PubMed: 24778174]
16. Cui Y, Xie X, Jia F, He J, Li Z, Fu M, Hao H, Liu Y, Liu JZ, Cowan PJ, Zhu H, Sun Q, Liu Z. Ambient fine particulate matter induces apoptosis of endothelial progenitor cells through reactive oxygen species formation. Cell Physiol Biochem. 2015; 35:353–363. [PubMed: 25591776]
17. Dabkowski ER, Baseler WA, Williamson CL, Powell M, Razunguzwa TT, Frisbee JC, Hollander JM. Mitochondrial dysfunction in the type 2 diabetic heart is associated with alterations in spatially distinct mitochondrial proteomes. Am J Physiol Heart Circ Physiol. 2010; 299:H529–H540. [PubMed: 20543078]
18. Dabkowski ER, Williamson CL, Bukowski VC, Chapman RS, Leonard SS, Peer CJ, Callery PS, Hollander JM. Diabetic cardiomyopathy-associated dysfunction in spatially distinct mitochondrial subpopulations. Am J Physiol Heart Circ Physiol. 2009; 296:H359–H369. [PubMed: 19060128]
19. Dabkowski ER, Williamson CL, Hollander JM. Mitochondria-specific transgenic overexpression of phospholipid hydroperoxide glutathione peroxidase (GPx4) attenuates ischemia/reperfusion-associated cardiac dysfunction. Free Radic Biol Med. 2008; 45:855–865. [PubMed: 18638546]
20. Deng X, Zhang F, Wang L, Rui W, Long F, Zhao Y, Chen D, Ding W. Airborne fine particulate matter induces multiple cell death pathways in human lung epithelial cells. Apoptosis. 2014; 19:1099–1112. [PubMed: 24722831]
21. Dockery DW, Pope CA 3rd, Xu X, Spengler JD, Ware JH, Fay ME, Ferris BG Jr, Speizer FE. An association between air pollution and mortality in six US cities. N Engl J Med. 1993; 329:1753–1759. [PubMed: 8179653]
22. Dominici F, McDermott A, Zeger SL, Samet JM. National maps of the effects of particulate matter on mortality: exploring geographical variation. Environ Health Perspect. 2003; 111:39–44. [PubMed: 12515677]
23. Donaldson K, Stone V. Current hypotheses on the mechanisms of toxicity of ultrafine particles. Ann Ist Super Sanita. 2003; 39:405–410. [PubMed: 15098562]
24. Dye JA, Lehmann JR, McGee JK, Winsett DW, Ledbetter AD, Everitt JI, Ghio AJ, Costa DL. Acute pulmonary toxicity of particulate matter filter extracts in rats: coherence with epidemiologic studies in Utah Valley residents. Environ Health Perspect. 2001; 109(Suppl 3):395–403. [PubMed: 11427389]
26. Elder A, Oberdorster G. Translocation and effects of ultrafine particles outside of the lung. Clin Occup Environ Med. 2006; 5:785–796. [PubMed: 17110292]
28. Esch L, Hendryx M. Chronic cardiovascular disease mortality in mountaintop mining areas of central Appalachian states. J Rural Health. 2011; 27:350–357. [PubMed: 21967378]

29. Farina F, Sancini G, Mantecca P, Gallinotti D, Camatini M, Palestini P. The acute toxic effects of particulate matter in mouse lung are related to size and season of collection. Toxicol Lett. 2011; 202:209–217. [PubMed: 21371539]
30. Gorr MW, Velten M, Nelin TD, Youtz DJ, Sun Q, Wold LE. Early life exposure to air pollution induces adult cardiac dysfunction. Am J Physiol Heart Circ Physiol. 2014; 307:H1353–H1360. [PubMed: 25172901]
31. Halestrap AP. What is the mitochondrial permeability transition pore? J Mol Cell Cardiol. 2009; 46:821–831. [PubMed: 19265700]
32. Hao Y, Jackson JR, Wang Y, Edens N, Pereira SL, Alway SE. β-Hydroxy-β-methylbutyrate reduces myonuclear apoptosis during recovery from hind limb suspension-induced muscle fiber atrophy in aged rats. Am J Physiol Regul Integr Comp Physiol. 2011; 301:R701–R715. [PubMed: 21697520]
33. Hartz AM, Bauer B, Block ML, Hong JS, Miller DS. Diesel exhaust particles induce oxidative stress, proinflammatory signaling, and P-glycoprotein up-regulation at the blood-brain barrier. FASEB J. 2008; 22:2723–2733. [PubMed: 18474546]
34. Hollander JM, Thapa D, Shepherd DL. Physiological and structural differences in spatially distinct subpopulations of cardiac mitochondria: influence of cardiac pathologies. Am J Physiol Heart Circ Physiol. 2014; 307:H1–H14. [PubMed: 24778166]
35. Jones T, Blackmore P, Leach M, Berube K, Sexton K, Richards R. Characterisation of airborne particles collected within and proximal to an opencast coalmine: South Wales, UK. Environ Monit Assess. 2002; 75:293–312. [PubMed: 12004982]
36. Knuckles TL, Stapleton PA, Minarchick VC, Esch L, McCawley M, Hendryx M, Nurkiewicz TR. Air pollution particulate matter collected from an Appalachian mountaintop mining site induces microvascular dysfunction. Microcirculation. 2013; 20:158–169. [PubMed: 22963349]
37. Kodavanti UP, Moyer CF, Ledbetter AD, Schladweiler MC, Costa DL, Hauser R, Christiani DC, Nyska A. Inhaled environmental combustion particles cause myocardial injury in the Wistar Kyoto rat. Toxicol Sci. 2003; 71:237–245. [PubMed: 12563109]
38. Kreyling WG, Semmler-Behnke M, Moller W. Ultrafine particle-lung interactions: does size matter? J Aerosol Med. 2006; 19:74–83. [PubMed: 16551218]
39. Kurth L, Kolker A, Engle M, Geboy N, Hendryx M, Orem W, McCawley M, Crosby L, Tatu C, Varonka M, DeVera C. Atmospheric particulate matter in proximity to mountaintop coal mines: sources and potential environmental and human health impacts. Environ Geochem Health. 2014; 37:529–544. [PubMed: 25537164]
40. Kurth LM, McCawley M, Hendryx M, Lusk S. Atmospheric particulate matter size distribution and concentration in West Virginia coal mining and non-mining areas. J Expo Sci Environ Epidemiol. 2014; 24:405–411. [PubMed: 24549227]
41. Kuznetsov AV, Troppmair J, Sucher R, Hermann M, Saks V, Margreiter R. Mitochondrial subpopulations and heterogeneity revealed by confocal imaging: possible physiological role? Biochim Biophys Acta. 2006; 1757:686–691. [PubMed: 16712778]
42. Kwong JQ, Molkentin JD. Physiological and pathological roles of the mitochondrial permeability transition pore in the heart. Cell Metab. 2015; 21:206–214. [PubMed: 25651175]
43. Laemmli UK. Cleavage of structural proteins during the assembly of the head of bacteriophage T4. Nature. 1970; 227:680–685. [PubMed: 5432063]
44. Langrish JP, Bosson J, Unosson J, Muala A, Newby DE, Mills NL, Blomberg A, Sandstrom T. Cardiovascular effects of particulate air pollution exposure: time course and underlying mechanisms. J Intern Med. 2012; 272:224–239. [PubMed: 22724512]
45. Minarchick VC, Stapleton PA, Fix NR, Leonard SS, Sabolsky EM, Nurkiewicz TR. Intravenous and gastric cerium dioxide nanoparticle exposure disrupts microvascular smooth muscle signaling. Toxicol Sci. 2014; 144:77–89. [PubMed: 25481005]
46. Minarchick VC, Stapleton PA, Porter DW, Wolfarth MG, Ciftyurek E, Barger M, Sabolsky EM, Nurkiewicz TR. Pulmonary cerium dioxide nanoparticle exposure differentially impairs coronary and mesenteric arteriolar reactivity. Cardiovasc Toxicol. 2013; 13:323–337. [PubMed: 23645470]
47. Nelin TD, Joseph AM, Gorr MW, Wold LE. Direct and indirect effects of particulate matter on the cardiovascular system. Toxicol Lett. 2012; 208:293–299. [PubMed: 22119171]

48. Nemmar A, Vanbilloen H, Hoylaerts MF, Hoet PH, Verbruggen A, Nemery B. Passage of intratracheally instilled ultrafine particles from the lung into the systemic circulation in hamster. Am J Respir Crit Care Med. 2001; 164:1665–1668. [PubMed: 11719307]
49. Nurkiewicz TR, Porter DW, Barger M, Castranova V, Boegehold MA. Particulate matter exposure impairs systemic microvascular endothelium-dependent dilation. Environ Health Perspect. 2004; 112:1299–1306. [PubMed: 15345343]
50. Nurkiewicz TR, Porter DW, Barger M, Millecchia L, Rao KM, Marvar PJ, Hubbs AF, Castranova V, Boegehold MA. Systemic microvascular dysfunction and inflammation after pulmonary particulate matter exposure. Environ Health Perspect. 2006; 114:412–419. [PubMed: 16507465]
51. Nurkiewicz TR, Porter DW, Hubbs AF, Stone S, Moseley AM, Cumpston JL, Goodwill AG, Frisbee SJ, Perrotta PL, Brock RW, Frisbee JC, Boegehold MA, Frazer DG, Chen BT, Castranova V. HEI Health Review Committee. Pulmonary particulate matter and systemic microvascular dysfunction. Res Rep Health Eff Inst. 2011:3–48. [PubMed: 22329339]
52. Oberdorster G, Sharp Z, Atudorei V, Elder A, Gelein R, Kreyling W, Cox C. Translocation of inhaled ultrafine particles to the brain. Inhal Toxicol. 2004; 16:437–445. [PubMed: 15204759]
53. Oberdorster G, Sharp Z, Atudorei V, Elder A, Gelein R, Lunts A, Kreyling W, Cox C. Extrapulmonary translocation of ultrafine carbon particles following whole-body inhalation exposure of rats. J Toxicol Environ Health A. 2002; 65:1531–1543. [PubMed: 12396867]
54. Palmer JW, Tandler B, Hoppel CL. Biochemical properties of subsarcolemmal and interfibrillar mitochondria isolated from rat cardiac muscle. J Biol Chem. 1977; 252:8731–8739. [PubMed: 925018]
55. Palmer MA, Bernhardt ES, Schlesinger WH, Eshleman KN, Foufoula-Georgiou E, Hendryx MS, Lemly AD, Likens GE, Loucks OL, Power ME, White PS, Wilcock PR. Science and regulation. Mountaintop mining consequences. Science. 2010; 327:148–149. [PubMed: 20056876]
56. Parrish AB, Freel CD, Kornbluth S. Cellular mechanisms controlling caspase activation and function. Cold Spring Harb Perspect Biol. 2013; 5:a008672. [PubMed: 23732469]
57. Peng RD, Dominici F, Pastor-Barriuso R, Zeger SL, Samet JM. Seasonal analyses of air pollution and mortality in 100 US cities. Am J Epidemiol. 2005; 161:585–594. [PubMed: 15746475]
58. Peretz A, Peck EC, Bammler TK, Beyer RP, Sullivan JH, Trenga CA, Srinouanprachnah S, Farin FM, Kaufman JD. Diesel exhaust inhalation and assessment of peripheral blood mononuclear cell gene transcription effects: an exploratory study of healthy human volunteers. Inhal Toxicol. 2007; 19:1107–1119. [PubMed: 17987463]
59. Perez CM, Hazari MS, Farraj AK. Role of autonomic reflex arcs in cardiovascular responses to air pollution exposure. Cardiovasc Toxicol. 2015; 15:69–78. [PubMed: 25123706]
60. Pope CA 3rd, Dockery DW. Health effects of fine particulate air pollution: lines that connect. J Air Waste Manag Assoc. 2006; 56:709–742. [PubMed: 16805397]
61. Pope CA 3rd, Thun MJ, Namboodiri MM, Dockery DW, Evans JS, Speizer FE, Heath CW Jr. Particulate air pollution as a predictor of mortality in a prospective study of US adults. Am J Respir Crit Care Med. 1995; 151:669–674. [PubMed: 7881654]
62. Quay JL, Reed W, Samet J, Devlin RB. Air pollution particles induce IL-6 gene expression in human airway epithelial cells via NF-kappaB activation. Am J Respir Cell Mol Biol. 1998; 19:98–106. [PubMed: 9651185]
63. Ruckerl R, Phipps RP, Schneider A, Frampton M, Cyrys J, Oberdorster G, Wichmann HE, Peters A. Ultrafine particles and platelet activation in patients with coronary heart disease—results from a prospective panel study. Part Fibre Toxicol. 2007; 4:1. [PubMed: 17241467]
64. Samet JM, Dominici F, Curriero FC, Coursac I, Zeger SL. Fine particulate air pollution and mortality in 20 US cities, 1987–1994. N Engl J Med. 2000; 343:1742–1749. [PubMed: 11114312]
65. Shimada A, Kawamura N, Okajima M, Kaewamatawong T, Inoue H, Morita T. Translocation pathway of the intratracheally instilled ultrafine particles from the lung into the blood circulation in the mouse. Toxicol Pathol. 2006; 34:949–957. [PubMed: 17178695]
66. Skulachev VP. Mitochondrial filaments and clusters as intracellular power-transmitting cables. Trends Biochem Sci. 2001; 26:23–29. [PubMed: 11165513]
67. Stapleton PA, Minarchick VC, Cumpston AM, McKinney W, Chen BT, Sager TM, Frazer DG, Mercer RR, Scabilloni J, Andrew ME, Castranova V, Nurkiewicz TR. Impairment of coronary

arteriolar endothelium-dependent dilation after multi-walled carbon nanotube inhalation: a time-course study. Int J Mol Sci. 2012; 13:13781–13803. [PubMed: 23203034]

68. Tamagawa E, Bai N, Morimoto K, Gray C, Mui T, Yatera K, Zhang X, Xing L, Li Y, Laher I, Sin DD, Man SF, van Eeden SF. Particulate matter exposure induces persistent lung inflammation and endothelial dysfunction. Am J Physiol Lung Cell Mol Physiol. 2008; 295:L79–L85. [PubMed: 18469117]
69. Tankersley CG, Champion HC, Takimoto E, Gabrielson K, Bedja D, Misra V, El-Haddad H, Rabold R, Mitzner W. Exposure to inhaled particulate matter impairs cardiac function in senescent mice. Am J Physiol Regul Integr Comp Physiol. 2008; 295:R252–R263. [PubMed: 18448608]
70. Thapa D, Nichols CE, Lewis SE, Shepherd DL, Jagannathan R, Croston TL, Tveter KJ, Holden AA, Baseler WA, Hollander JM. Transgenic overexpression of mitofilin attenuates diabetes mellitus-associated cardiac and mitochondria dysfunction. J Mol Cell Cardiol. 2015; 79:212–223. [PubMed: 25463274]

70a. US Energy Information Administration. Annual Energy Outlook 2010. Washington DC: US Energy Information Administration; 2010.

70b. US Energy Information Administration. Annual Coal Report 2013. Washington, DC: US Energy Information Administration; 2015.

70c. US Environmental Protection Agency. Air Quality Criteria for Particulate Matter (Final Report, Oct 2004). Washington, DC: US Environmental Protection Agency; 2004.

71. van Eeden SF, Tan WC, Suwa T, Mukae H, Terashima T, Fujii T, Qui D, Vincent R, Hogg JC. Cytokines involved in the systemic inflammatory response induced by exposure to particulate matter air pollutants [PM(10)]. Am J Respir Crit Care Med. 2001; 164:826–830. [PubMed: 11549540]
72. Van Hee VC, Adar SD, Szpiro AA, Barr RG, Bluemke DA, Diez Roux AV, Gill EA, Sheppard L, Kaufman JD. Exposure to traffic and left ventricular mass and function: the Multi-Ethnic Study of Atherosclerosis. Am J Respir Crit Care Med. 2009; 179:827–834. [PubMed: 19164703]
73. Veronesi B, Oortgiesen M, Carter JD, Devlin RB. Particulate matter initiates inflammatory cytokine release by activation of capsaicin and acid receptors in a human bronchial epithelial cell line. Toxicol Appl Pharmacol. 1999; 154:106–115. [PubMed: 9882597]
74. Wang Y, Hao Y, Alway SE. Suppression of GSK-3beta activation by M-cadherin protects myoblasts against mitochondria-associated apoptosis during myogenic differentiation. J Cell Sci. 2011; 124:3835–3847. [PubMed: 22114306]
75. WHO. Ambient (Outdoor) Air Quality And Health. Geneva, Switzerland: World Health Organization; 2014.
76. WHO. World Health Report 2002. Geneva, Switzerland: World Health Organization; 2002.
77. Williamson CL, Dabkowski ER, Baseler WA, Croston TL, Alway SE, Hollander JM. Enhanced apoptotic propensity in diabetic cardiac mitochondria: influence of subcellular spatial location. Am J Physiol Heart Circ Physiol. 2010; 298:H633–H642. [PubMed: 19966057]
78. Williamson CL, Dabkowski ER, Dillmann WH, Hollander JM. Mitochondria protection from hypoxia/reoxygenation injury with mitochondria heat shock protein 70 overexpression. Am J Physiol Heart Circ Physiol. 2008; 294:H249–H256. [PubMed: 17982016]
79. Wilson WE, Suh HH. Fine particles and coarse particles: concentration relationships relevant to epidemiologic studies. J Air Waste Manag Assoc. 1997; 47:1238–1249. [PubMed: 9448515]
80. Wold LE, Ying Z, Hutchinson KR, Velten M, Gorr MW, Velten C, Youtz DJ, Wang A, Lucchesi PA, Sun Q, Rajagopalan S. Cardiovascular remodeling in response to long-term exposure to fine particulate matter air pollution. Circ Heart Fail. 2012; 5:452–461. [PubMed: 22661498]
81. Woolley SM, Meacham SL, Balmert LC, Talbott EO, Buchanich JM. Comparison of mortality disparities in central Appalachian coal- and non-coal-mining counties. J Occup Environ Med. 2015; 57:687–694. [PubMed: 25806416]
82. Yan YH, Huang CH, Chen WJ, Wu MF, Cheng TJ. Effects of diesel exhaust particles on left ventricular function in isoproterenol-induced myocardial injury and healthy rats. Inhal Toxicol. 2008; 20:199–203. [PubMed: 18236234]
83. Yuan S, Akey CW. Apoptosome structure, assembly, and procaspase activation. Structure. 2013; 21:501–515. [PubMed: 23561633]

84. Zanobetti A, Schwartz J. The effect of fine and coarse particulate air pollution on mortality: a national analysis. Environ Health Perspect. 2009; 117:898–903. [PubMed: 19590680]

85. Zhang J, Ghio AJ, Chang W, Kamdar O, Rosen GD, Upadhyay D. Bim mediates mitochondria-regulated particulate matter-induced apoptosis in alveolar epithelial cells. FEBS Lett. 2007; 581:4148–4152. [PubMed: 17716672]

86. Zhou B, Liang G, Qin H, Peng X, Huang J, Li Q, Qing L, Zhang L, Chen L, Ye L, Niu P, Zou Y. p53-dependent apoptosis induced in human bronchial epithelial (16-HBE) cells by PM2.5 sampled from air in Guangzhou, China. Toxicol Mech Methods. 2014; 24:552–559. [PubMed: 25133668]

87. Zhou L, O'Rourke B. Cardiac mitochondrial network excitability: insights from computational analysis. Am J Physiol Heart Circ Physiol. 2012; 302:H2178–H2189. [PubMed: 22427517]

88. Zullig KJ, Hendryx M. A comparative analysis of health-related quality of life for residents of US counties with and without coal mining. Public Health Rep. 2010; 125:548–555. [PubMed: 20597455]

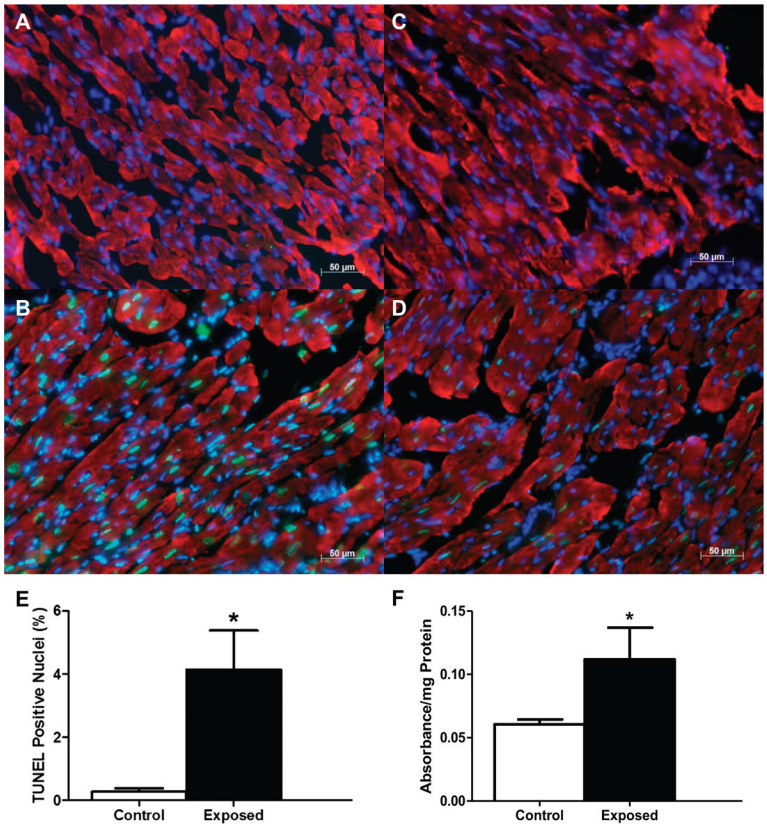

Fig. 1.

Cardiac apoptotic index following mountaintop removal mining particulate matter (PM_{MTM}) exposure. Representative fluorescent images of cardiac tissue. *A*: negative control with exclusion of TdT enzyme. *B*: positive control with inclusion of DNase I. *C*: control with vehicle instillation. *D*: exposure with PM_{MTM} instillation. DAPI-stained nuclei are indicated in blue, whereas terminal dUTP nick-end labeling (TUNEL)-positive nuclei are shown in green, and red indicates heavy chain cardiac myosin. Scale bar = 50 μm. *E*: apoptotic index was calculated as the percentage of total cardiomyocyte nuclei that were TUNEL-positive nuclei. Values are means ± SE; $n = 3$ for each group. *F*: relative cytosolic histone concentrations determined by ELISA on left ventricular tissue from control and PM_{MTM}-exposed animals. Values are means ± SE; $n = 5$ for each group. *$P < 0.05$ for control vs. exposed.

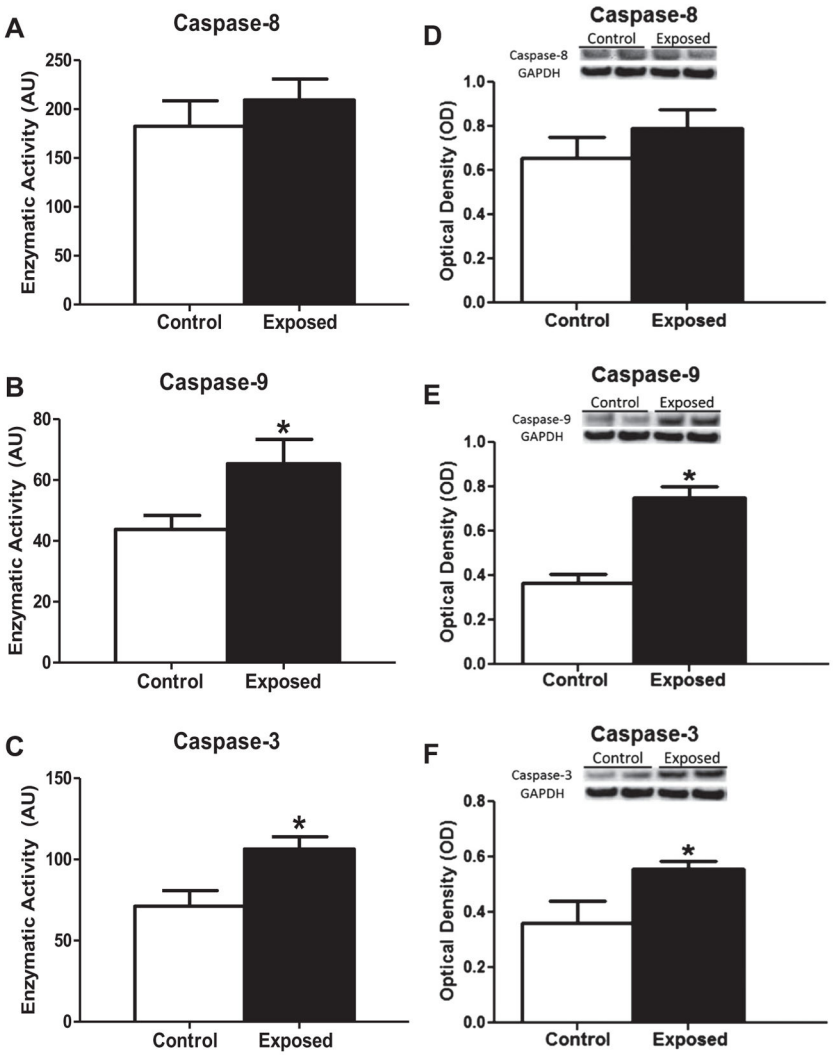

Fig. 2.

Cardiac caspase activities and content following PM_{MTM} exposure. Fluorometric analysis of enzymatic activities of caspase-8 (*A*), caspase-9 (*B*), and caspase-3 (*C*) from the cytosol of rat left ventricles exposed by instillation to either vehicle control or PM_{MTM}. Data are expressed as arbitrary units (AU). Relative protein contents of activated caspases from cytosolic fractions from left ventricles of rats exposed by instillation to either vehicle control or PM_{MTM}. Representative Western blots (*top*) and densitometric analyses (*bottom*) for total protein content of caspase-8 (*D*), caspase-9 (*E*), and caspase-3 (*F*). All Western blots are expressed per GAPDH levels. Values are means ± SE; $n = 6$ for each group. *$P < 0.05$ for control vs. exposed.

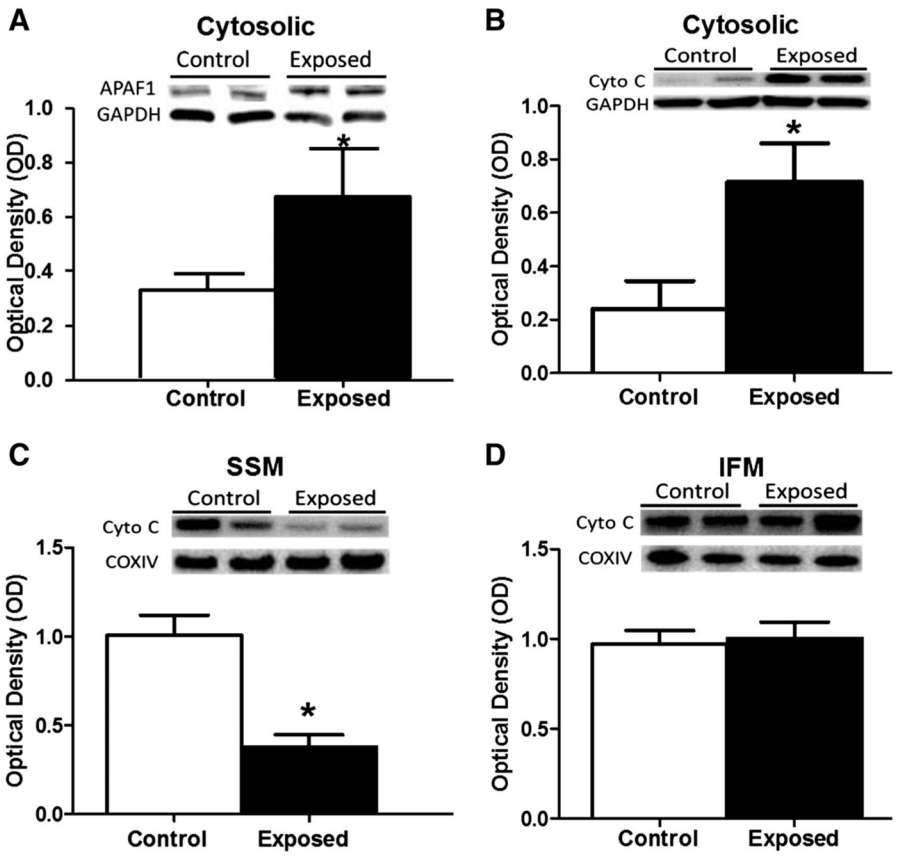

Fig. 3.

Apoptosome constituent contents. Relative protein contents of apoptosome constituents from cytosol and isolated mitochondrial subpopulations from left ventricles of rats exposed by instillation to either vehicle control or PM_{MTM}. Representative Western blots (*top*) and densitometric analyses (*bottom*) for total protein content of cytosolic apoptosis protease activating factor 1 (APAF1) (*A*), cytosolic cytochrome *c* (Cyto C) (*B*), cytochrome *c* in the subsarcolemmal mitochondria (SSM) (*C*), and cytochrome *c* in the interfibrillar mitochondria (IFM) (*D*). Cytosolic proteins (*A* and *B*) were expressed per GAPDH levels, whereas mitochondrial analyses (*C* and *D*) were expressed per COX IV levels. Values are means ± SE; $n = 8$ for each group. *$P < 0.05$ for control vs. exposed.

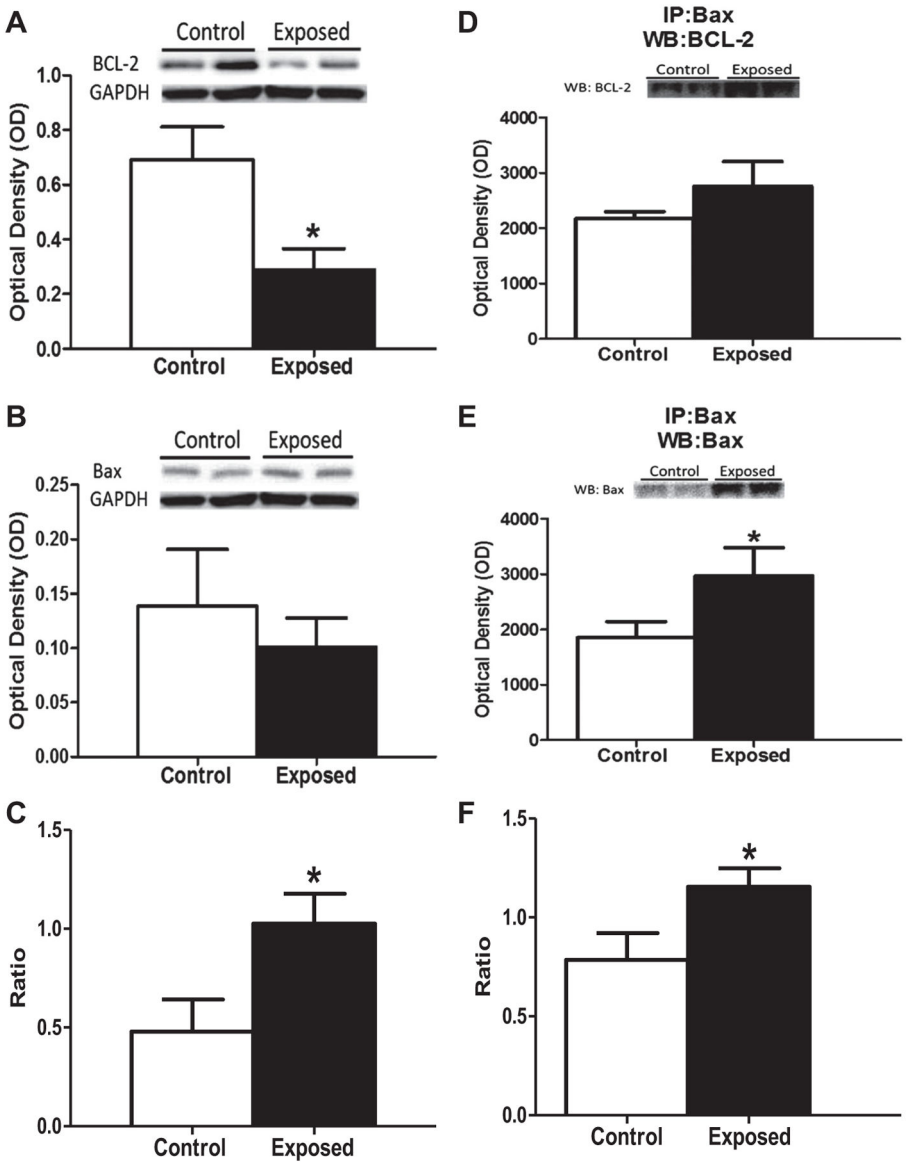

Fig. 4.

Bcl-2-associated X protein (Bax) and B-cell lymphoma 2 (Bcl-2) protein contents. Relative protein contents of total cell markers of apoptosis from left ventricles of rats exposed by instillation to either vehicle control or PM_{MTM}. Representative immunoblots (*top*) and densitometric analyses (*bottom*) for cytosolic Bax (*A*) and Bcl-2 (*B*). *C*: ratio of densitometric analysis of Bax to Bcl-2. Western blots are expressed per GAPDH levels. Immunoblots from coimmunoprecipitation with Bax suggesting the formation of hetero-or homodimers with Bcl-2 (*D*) or Bax (*E*). Ratio of densitometric analysis of Bax dimers with Bax to Bcl-2 (*F*). Values are means ± SE; $n = 8$ for each group, $^*P < 0.05$ for control vs. exposed.

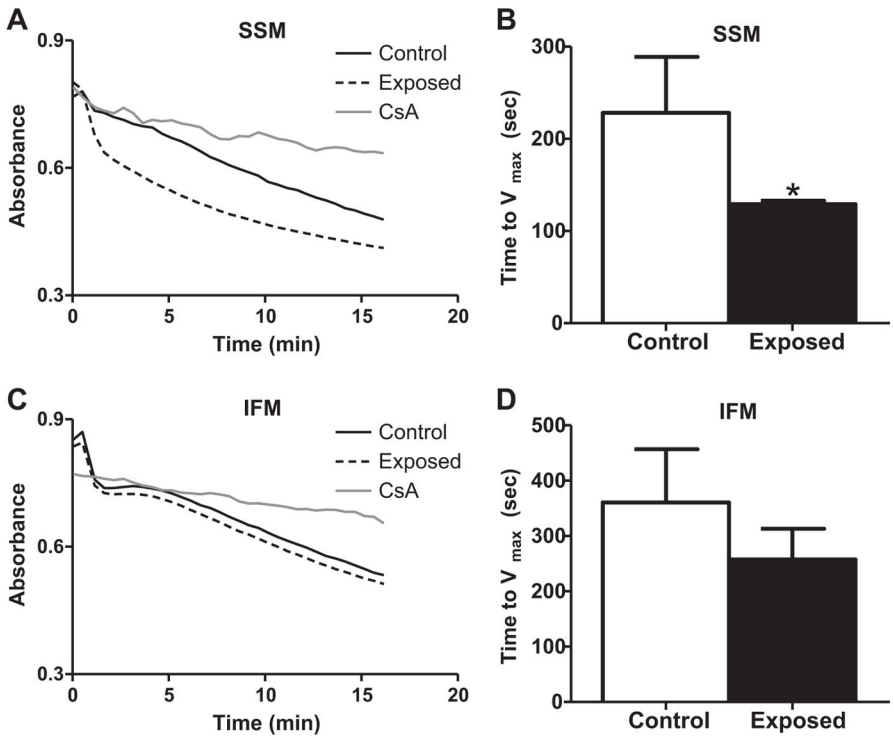

Fig. 5.

Mitochondrial permeability transition pore (mPTP) opening propensity. mPTP opening propensity from left ventricles of rats exposed by instillation to either vehicle control or PM_{MTM}. Spectrophotometric analysis of mPTP opening propensity using the exogenous oxidant tert-butyl hydroperoxide (t-BuOOH) to induce mitochondrial swelling. Time to V_{max} was assessed over a 15-min time period. Representative absorbance plots for SSM (*A*) and IFM (*C*). Solid lines represent control, dashed lines represent exposed, and dotted lines represent the internal control, cyclosporine A (CsA) treatment. V_{max} data graphed for SSM (*B*) and IFM (*D*). Values are means ± SE; $n = 6$ for each group. *$P < 0.05$ for control vs. exposed.

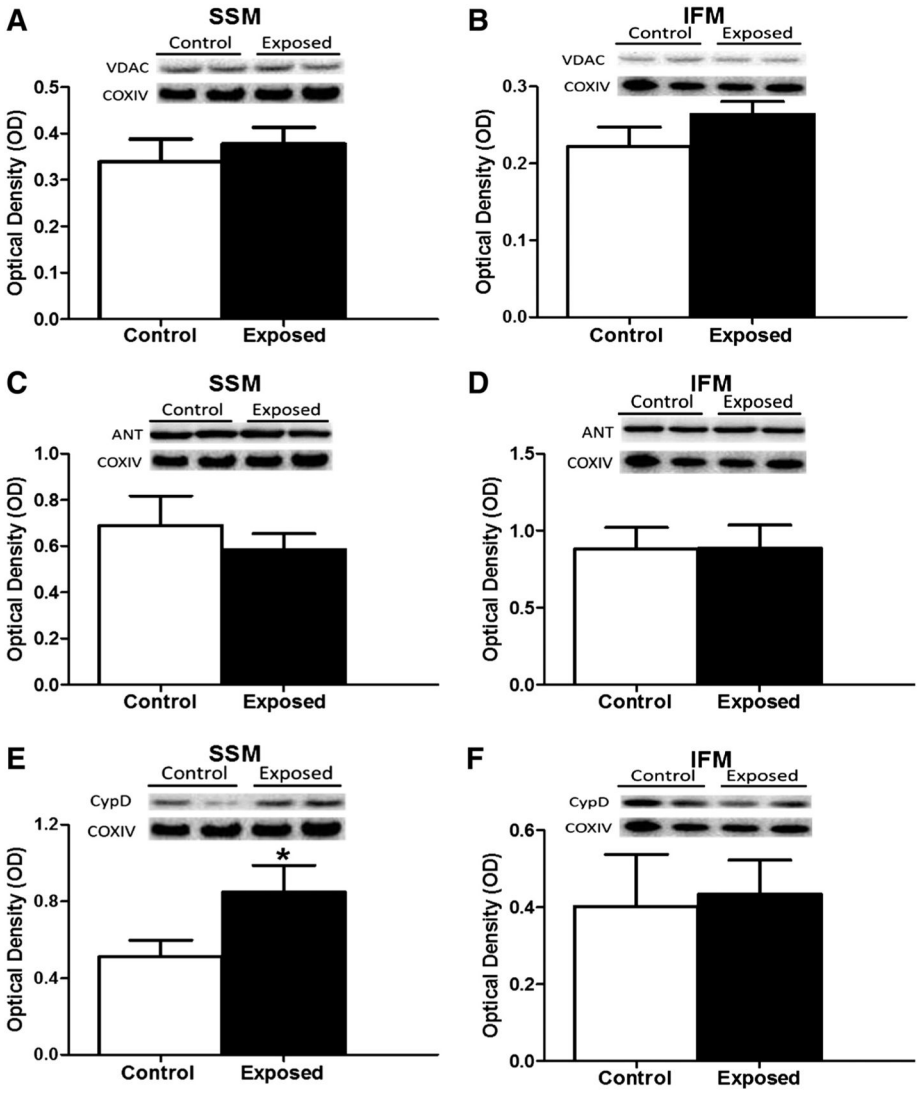

Fig. 6.

mPTP components. Relative protein content assessed by Western blotting of putative members of the mPTP from left ventricles of rats exposed by instillation to either vehicle control or PM_{MTM}. Representative Western blots (*top*) and densitometric analyses (*bottom*) for total voltage-dependent anion channel (VDAC) in SSM (*A*) and in IFM (*B*), adenine nucleotide translocase (ANT) in SSM (*C*) and IFM (*D*), and cyclophilin D (CypD) in SSM (*E*) and IFM (*F*). All Western blots are expressed per COX IV levels. Values are means ± SE; $n = 8$ for each group. $^*P < 0.05$ for control vs. exposed.

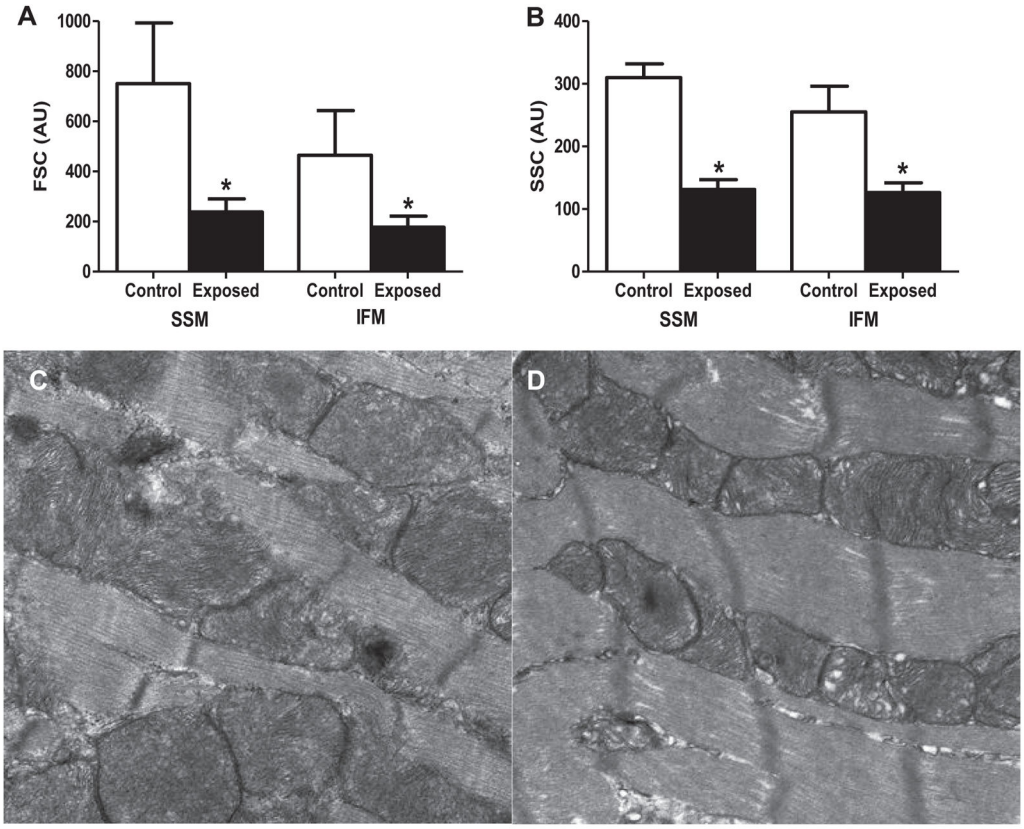

Fig. 7.

Mitochondrial morphological assessment. Relative size and internal complexity were analyzed using mitotracker deep red 633 and flow cytometry. *A*: analysis of cardiac SSM and IFM size (forward scatter, FSC) in control and exposed mitochondria subpopulations. *B*: analysis of cardiac SSM and IFM internal complexity (side scatter, SSC) in control and exposed mitochondrial subpopulations. Representative electron micrographs of left ventricle tissue from control (*C*) and PM_{MTM} exposed (*D*) animals. Values for both FSC and SSC are expressed as AU ± SE; $n = 8$ for each group. *$P < 0.05$ for control vs. exposed.

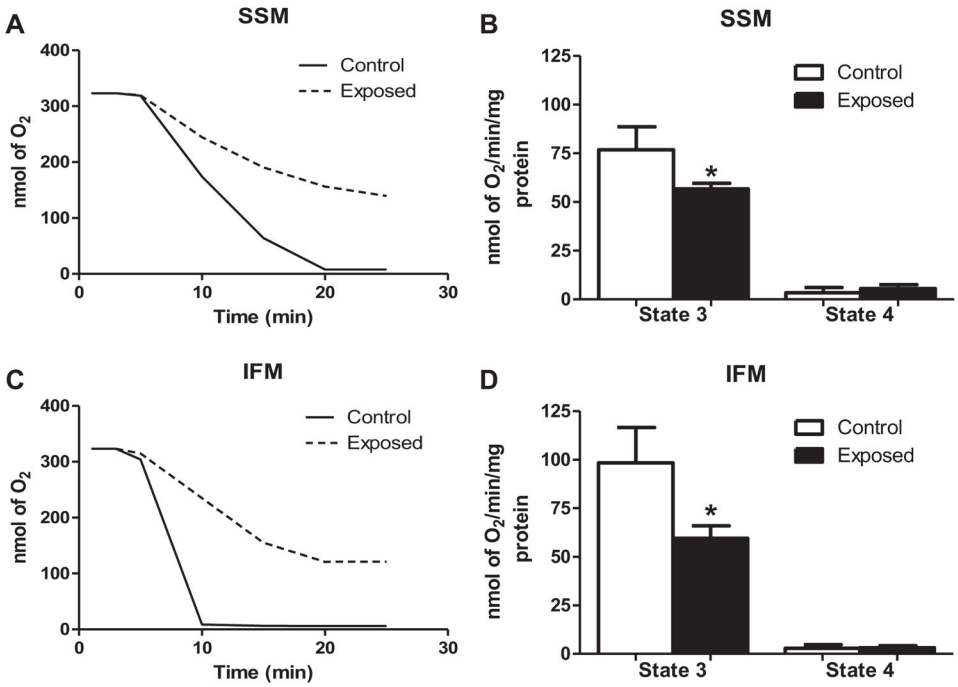

Fig. 8.

Mitochondrial respiratory capacity. Representative polarographic traces of oxygen consumption following addition of glutamate and malate to SSM (*A*) and IFM (*C*). Solid line traces represent mitochondria from control, and dashed line traces represent mitochondria from PM_{MTM}-exposed animals. Summary analyses of state 3 and state 4 respiration rates from trace measurements of SSM (*B*) and IFM (*D*). Respiration rates are expressed in nmol·min^{-1}·mg protein^{-1}. Values are means ± SE; $n = 6$ for each group. *$P < 0.05$ for control vs. exposed animals.

Table 1

M-mode echocardiographic measurements

Parameter	Control Average ± SE	Exposed Average ± SE
Heart weight, mg	743.00 ± 39.39	837.00 ± 51.00
Body weight, g	299.63 ± 8.94	288.5 ± 1.50
Heart weight:body weight	2.51 ± 0.18	2.90 ± 0.19
Heart rate, beats/min	416.60 ± 10.38	403.54 ± 10.05
Systolic diameter, mm	2.29 ± 0.09	2.71 ± 0.18*
Diastolic diameter, mm	5.62 ± 0.08	5.84 ± 0.18
Systolic volume, μl	18.66 ± 1.97	29.46 ± 5.08*
Diastolic volume, μl	155.39 ± 5.22	171.61 ± 12.12
Stroke volume, μl	136.73 ± 5.54	142.15 ± 8.84
Ejection fraction, %	87.88 ± 1.25	83.53 ± 1.98*
Fractional shortening, %	59.16 ± 1.76	53.89 ± 2.09*
Cardiac output, ml/min	57.15 ± 3.16	57.33 ± 3.79

Values are means ± SE; $n = 10$ for each group.

* $P < 0.05$ for control vs. exposed animals.